Electronic Supplementary Information (ESI) for

Impact of π-Conjugation and Fluorination on the Sensing Performance of 1,6-Pyrene Covalent Triazine Frameworks

M. Carmen Borrallo-Aniceto,[a] Beatriz Fuerte-Díez,[a] Laura González-Aguilera,[a] M. Luisa Ferrer,[a] M. Pilar Lillo,[b] Andreas Mavrandonakis,[a] Urbano Díaz,[c] Eva M. Maya,[a] * Marta Iglesias[a,]*

[a]Instituto de Ciencia de Materiales de Madrid. CSIC. C/ Sor Juana Inés de la Cruz, 3, 28049. Madrid, Spain.

[b]Instituto de Química Física Blas Cabrera. CSIC. C/ Serrano, 119, 28006. Madrid Spain.

[c]Instituto de Tecnología Química, Universitat Politècnica de València, Consejo Superior de Investigaciones Científicas, Avenida de los Naranjos s/n, E-46022 Valencia, Spain

1. Materials and Characterization Methods

Warning! Nitroexplosives, as picric acid, are explosive and should be handled with proper protection measures.

Materials and Measurements. Picric acid (PA), nitrobenzene (NB), 4-nitrotoluene (4-NT), 1,4-dinitrobenzene (1,4-DNB), 2,4-dinitrotoluene (2,4-DNT), 2-nitroaniline (2-NA), 2-methyl-1-nitronaphthalene (2M-1-NN), 3-nitrobenzaldehyde (3-NBA) and 1-nitromethane (1-NM) were obtained from commercial sources. 1,6-dibromopyrene was purchased from commercial sources. 1,6-*bis*(Bpin)pyrene was synthesized according to literature procedures.[1]

All other reagents were obtained from commercial sources and employed without additional purification unless otherwise indicated. Solvents were dried by standard methods.

Nuclear magnetic resonance (NMR) spectra of molecular samples were recorded with a BRUKER AVANCE III HD 400 (Larmor frequencies of 400 for ^{1}H, ^{13}C and ^{19}F) for liquids and a Bruker AV400 WB spectrometer (Larmor frequencies of 400 and 100 MHz) using 4 mm MAS probes spinning at 10 kHz rate for ^{13}C solid-state MAS-NMR measurements. The ^{13}C CP-MAS spectra were obtained using 3.5 ms contact time and 4 s relaxation time. NMRs of the fluorinated molecules were uncoupled.

Fourier Infrared (ATR) spectra were recorded on an appliance type Perkin Elmer Spectrum Two with a Fourier Transformer.

Elemental analysis (%C, %N %H and %S) were determined in a TruSpec Micro Elemental CHN/CHNS LECO analyzer.

The **HR-MS** analysis was carried out by using an Agilent 1200 Series LC system coupled to a 6520 quadrupole-time of flight (QTOF) mass spectrometer. Acetonitrile: water (75:25, v:v) was used as mobile phase at 0.2 mL min^{-1}. The ionization source was an ESI interface working in the positive-ion mode or by APCI, Atmospheric Pressure Chemical Ionization.

Raman spectra were performed on samples placed on a microscope slide with a Renishaw inVia Raman microscope using irradiation at 514 nm.

The **microwave** oven used for the CTFs synthesis was ANTON PAAR MONOWAVE 300.

Thermogravimetric and differential thermal analyses (**TGA**) were conducted on a with a TA Instruments Model TA-Q500 analyzer. The samples were heated from 30 to 800 ºC under air atmosphere with a heating rate 10 ºC/min.

EPR spectra were recorded at 100k on a Bruker EMX-12 instrument operating in X band at 9.5GHz, modulation amplitude of 1G and modulation frequency of 100KHz.

Nitrogen adsorption isotherms were measured at 77 K using a Quantachrome surface and porosity analyzer. Prior to measurement, the samples were degassed for 16 hours at 120°C.

Specific surface areas were determined by N_2 adsorption-desorption at 77K and the pore distribution by DFT methods. Surface area was determined by the Brunauer–Emmett–Teller (BET) method. The **CO_2 gas adsorption** measurements were carried out using a Micromeritics ASAP 2010 instrument. The samples were degassed at 150ºC in high vacuum before measurements. The surface areas and pore volumes were determined via CO_2 adsorption at 273 K by the Dubinin-Astakhov method.

The morphology was analyzed by a Field Emission Scanning Electron Microscopy **SEM** model FEI Nova NanoSEM 230 equipped with an Energy Dispersive X-ray spectroscopy (EDAX) analyzer, EDAX SUTW equipment (Super Ultra-Thin Window). The samples were previously metallized with gold.

Transmission electron microscopy **(TEM)** was performed in a JEOL model JEM-1400Flash with a STEM detector. For the analysis, a small amount of the sample was dispersed in dichloromethane. Then, a drop was placed on a nickel grid and dried under a lamp for 2 h.

The C1s, N1s, F1s and survey spectra of **XPS** were recorded using a Thermo Scientific K-Alpha instrument. Monochromatic X-ray source Al Kα (1486.6 eV) was used for all samples and experiments. The X-Ray Monochromatic spot is 400 μm in diameter. Residual vacuum in the analysis chamber was maintained at around $6x10^{-10}$ mbar. We have also employed an electron flood gun to minimize surface charging (Charge compensation). The powder samples were fixed to the holder using a copper adhesive tape to ensure the powders are firmly attached during analysis.

Powder X-ray diffractograms were obtained in a Bruker D8 diffractometer with a Sol-X energy dispersive detector, working at 40 kV and 30 mA and employing CuKα (λ = 1.5418 Å) filtered radiation. The diffractograms were collected with a step size of 0.1º and exposure time of 0.5 s per step and a 2θ range of 3-50º.

Cyclic voltammetry was performed at 25ºC and a scan rate of 100 mV/s, under nitrogen atmosphere, using 0.1 M tetrabutylammonium hexafluorophosphate solution (NBu_4PF_6) in acetonitrile as electrolyte. A standard three-electrode electrochemical cell was employed with potentials referenced to an Ag/AgCl (3.5M KCl) reference electrode and platinum as counter electrode. The working electrode was a glassy carbon electrode (GCE) coated with a homogeneous hybrid paste. This paste was fabricated by mixing 3 mg of the material and 80μL drop of Nafion. Electrochemical impedance spectroscopy was obtained in the same way as for cyclic voltammetry. The hybrid paste was fabricated by mixing 5 mg of the material and 1mL of a mixture of ethanol Nafion (100/1).

Fluorescence spectra were logged on a Varian Cary Eclipse fluorescence spectrophotometer equipped with 1x1 cm quartz cuvette. The width of the excitation slit and the emission slit were set to 5.0 nm.

Picosecond time-resolved fluorescence intensity measurements were collected using a custom time-correlated single-photon counting system (TCSPC), including SPC630 card and SPCM data acquisition software (Becker and Hickl).[2,3]

The excitation light source was a LDH-P-C-375 diode laser head (PicoQuant, GmbH, Germany), operating at 372 nm. A laser repetition rate of 2.5 MHz was utilized. Total fluorescence intensity decays, $I(t) = I_m(t)$, were collected in the plane perpendicular to the vertical orientation of the linearly polarized excitation, at 90º to the excitation beam, through a 550 nm Schott cut-on Filter, and a Glan-Taylor polarizer set at the magic angle (54.7º, relative to the vertically polarized excitation beam), and detected by a microchannel plate (Hamamatsu R1564U-06) operating in the single-photon-counting, time-correlated mode.[2] Timing calibration was 24.4 ps per channel with 4096 channels of data obtained. Time-resolved measurements were performed in quartz cuvettes with a 5 × 5mm path-length. The temperature of the measurements was 20 ºC.

Fluorescence lifetime data analysis: Fluorescence lifetime parameters were determined by iterative convolution of the magic angle total intensity decays, $I_m(t)$, from nonlinear global least-squares multiexponential fitting analysis, using Globals for Spectroscopy program (LFD, Univ. California, Irvine CA):

$$I_m(t) = \sum_{i=1}^{n} a_i \cdot e^{\frac{-t}{\tau_i}}$$

Where a_i and τ_i are the amplitude and lifetime of each fluorescence decay component i, respectively. Four lifetimes were required for adequate fitting for all the samples.

The adequacy of the analyses was determined from the reduced weighted sum of squares of residuals, and visual inspection of the distribution of weighted residuals. It was found no variation in the lifetimes for each compound in absence and presence of the studied analytes. In these analyses, the lifetimes parameters were linked between compound and compound/analyte decays, for each compound.

The amplitude average lifetime $<\tau>$ was calculated from:

$$<\tau> = \left[\sum_{i=1}^{3} a_i \cdot \tau_i\right] \Big/ \sum_{i=1}^{3} a_i$$

In this calculation, only three lifetimes components were considered. A fourth lifetime of about 1 ps was assigned to the light scattering contribution of the sample suspensions.

2. Synthetic procedures

2.1 Synthesis of 1,6-pyrene-dinitriles

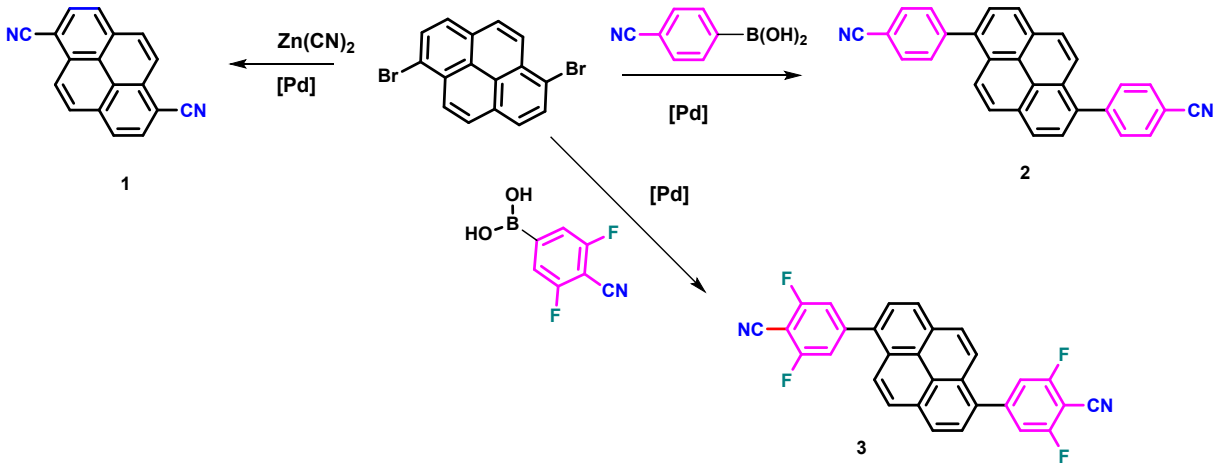

Scheme S1. Synthesis of dinitriles

2.1.1. Synthesis of pyrene-1,6-dicarbonitrile (1)

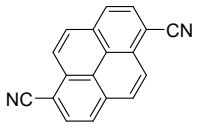

Dinitrile 1 was synthesised by an alternative method to that described in the literature.[4] In a 20 mL pressure tube, 6mL of DMA bubbled with nitrogen, 1,6-dibromopyrene (900 mg, 2.5 mmol, 1 eq.), 3 drops of polymethylhydrosiloxane (PMHS), zinc cyanide (323 mg, 2.75 mmol, 1.1eq) and 36 mg (0.05 mmol, 0.02 eq) [1,1′-*bis*(diphenylphosphino)ferrocene]dichloropalladium (II) was heated at 120ºC for 48h. The system was cooled to room temperature, is filtered, and washed with water, methanol and diethyl ether. The solid obtained is recrystallized in toluene. Pyrene-1,6-dicarbonitrile was obtained with a yield of 563 mg, 89%. **^{1}H-RMN** (300MHz, $CDCl_3$): 8.68 (d, J = 9.1Hz, 1H), 8.44 – 8.38 (m, 3H); **^{13}C NMR** (CP-MAS solid state) δ (ppm): 129.8 – 124.9, 118.8, 106.3 **MS** (MALDI-TOF) m/z: calcd. For $C_{18}H_8N_2$, 252.069; found 252.0683 (M^-). **FT-IR (ATR)** (cm^{-1}): 3043.8, 2223.2 (-C≡N), 1641.5, 1601.1, 0578.7, 1485.8, 1451.0, 1406.6, 1367.0, 1287.8, 1238.3, 1188.8, 1174.0, 1154.2, 1109.7, 1010.7, 971.1, 862.2, 837.5, 807.8, 733.5, 703.8, 684.0.

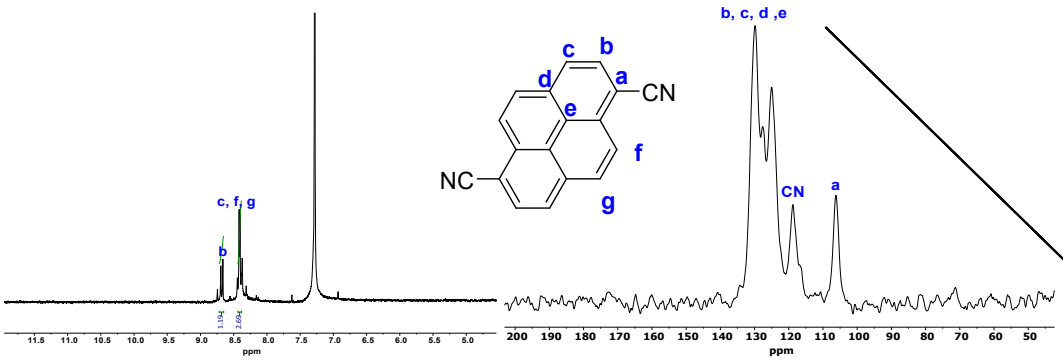

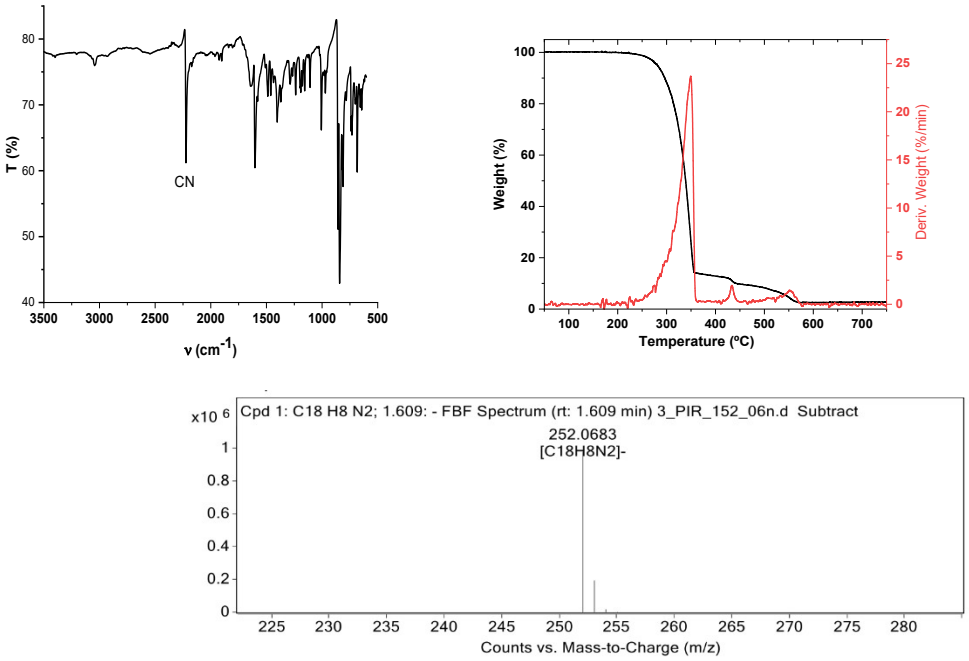

Figure S1. ^{1}H-NMR, ^{13}C-NMR, FT-IR, HRMS spectra and TGA of 1.

2.1.2 Synthesis of 4,4'-(pyrene-1,6-diyl)dibenzonitrile (2)[5]

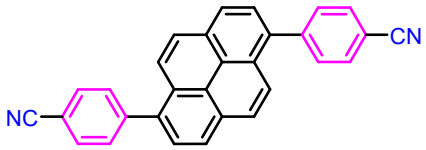

The mixture of 1,6-dibromopyrene (400mg, 1.1 mmol, 1eq), (4-cyanophenyl)boronic acid (490 mg, 3.3 mmol, 3eq), K_3PO_4 (1.1g, 5.5 mmol, 5eq) and 7mL of dimethylformamide was bubbled with N_2 for 10 min. Then, $Pd(PPh_3)_4$ (50 mg, 0.08 mmol, 7 mol %) was added at the pressure tube. The mixture was heated at 100°C for 48 h. The mixture was cooled to room temperature and the solution was filtered and the solid was washed with water, methanol and diethyl ether. Finally, the solid was recrystallised with DMA yielding 301 mg (67%) of a white solid. **^{1}H-RMN** (300MHz, $CDCl_3$): 8.27 (d, 2H, J=7.9 Hz), 8.11 (s, 4H), 7.98 (d, 2H, J=7.9 Hz), 7.88 (d, 4H, J=8.2 Hz), 7.76 (d, 4H, J=8.2 Hz), **^{13}C NMR (**CP-MAS solid state) δ (ppm): 144.7, 134.74, 132.55, 128.87, 127.17, 125.03, 122.73 (Ar), 110.3 (CN). **MS (MALDI-TOF) m/z:** calcd. For $C_{18}H_8N_2$, 404.131; found 404.1323 (M^-). **FT-IR (ATR)** (cm^{-1}): 3039.8, 2223.2 (-C≡N), 1948.2, 1888.0, 1776.3, 1647.3, 1604.3, 1509.8, 1449.6, 1406.6, 1380.9, 1320.7, 1269.1, 1200.3, 1183.2, 1157.4, 1105.8, 1028.4, 994.1, 976.9, 890.9, 856.5, 830.7, 813.6, 787.8, 753.4, 19.0, 658.8, 615.9.

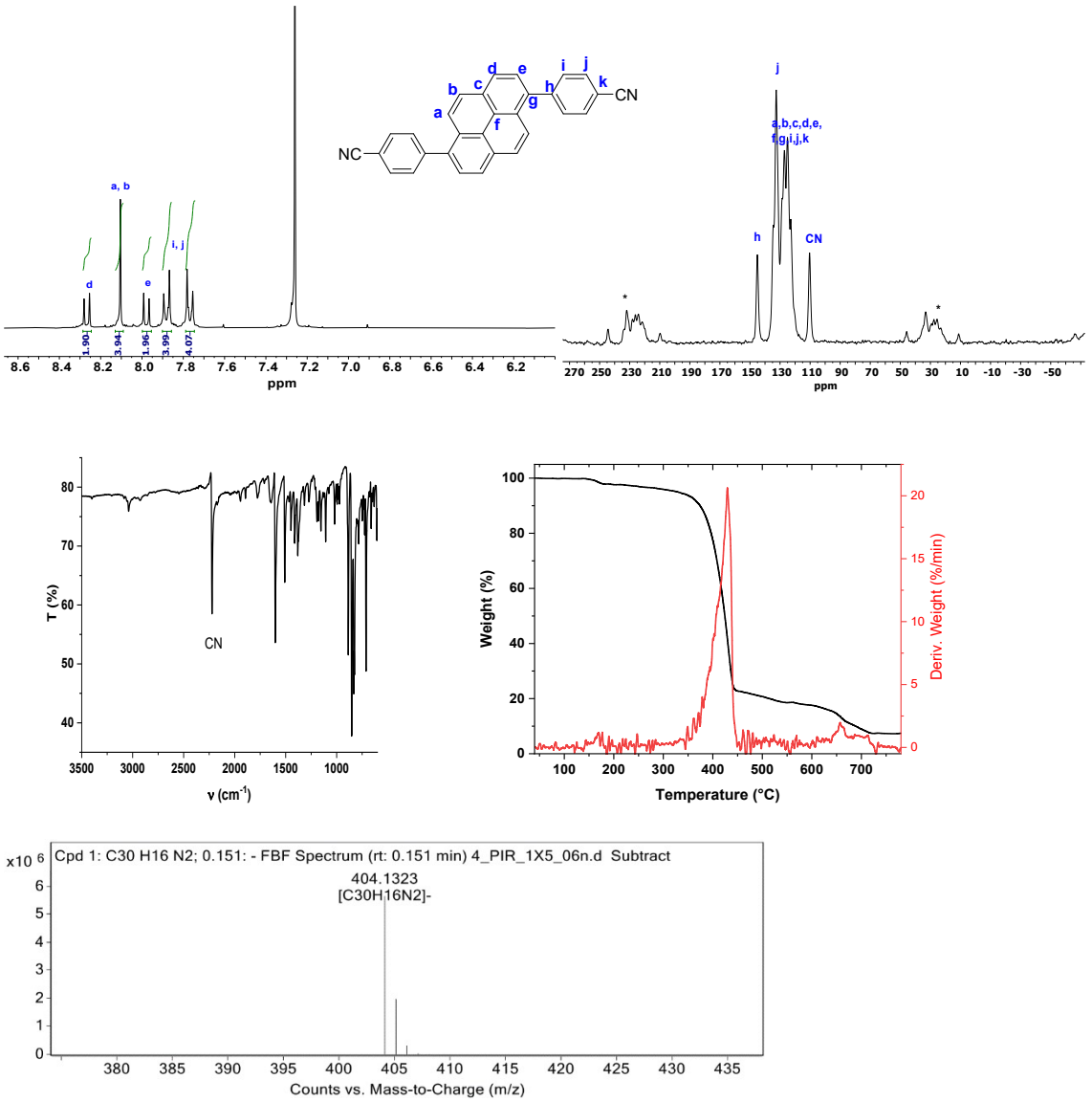

Figure S2. ^{1}H-NMR, ^{13}C-NMR, ATR-IR, HRMS spectra and TGA of **2**.

2.1.3 Synthesis of 4,4'-(pyrene-1,6-diyl)bis(2,6-difluorobenzonitrile) (3)

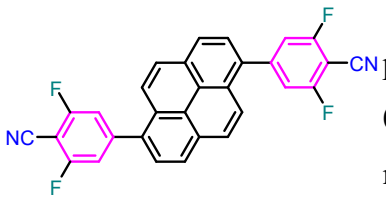

1,6-dibromopyrene (75 mg, 0.21 mmol), 4-cyano-3,5-difluoro-phenylboronic acid (85.7 mg, 0.47 mmol), $Pd(PPh_3)_2Cl_2$ (14.6 mg, 0.021 mmol) and K_2CO_3 (288 mg, 2.1 mmol) and a 4:1 THF: H_2O mixture was stirred at 85°C for 30h. The organic solvent was eliminated under vacuum and filtered. The product was washed with water, dichloromethane, methanol, ether and chloroform. The product was obtained as a green solid (71mg, yield = 72%). **^{1}H NMR** (hot DMSO, 300 MHz): δ 8.48 (d, J = 7.9 Hz, 2H), 8.34 (d, J = 9.4 Hz, 2H), 8.18 (dd, J = 17.5, 8.6 Hz, 4H), 7.81 (d, J = 9.2 Hz, 4H).**^{19}F NMR** (hot DMSO, 400 MHz): δ -105.57 (s, 4F). **^{13}C NMR** (CP-MAS solid state 400 MHz): δ 162.47, 147.25, 133.14 130.15, 124.09, 127.01,

116.10, 111.85, 91.41. **MS (MALDI-TOF) m/z**: calcd. For $C_{30}H_{12}F_4N_2$, 476.43; found 476.18. **FT-IR (ATR)** (cm^{-1}): 2238.1 (-C≡N), 1628.7, 1560.2, 1428.3, 1226.1, 1206.7, 1038.7 (C-F), 880.2, 853.3, 815.1, 735.4, 722.4, 687.0, 670.2.

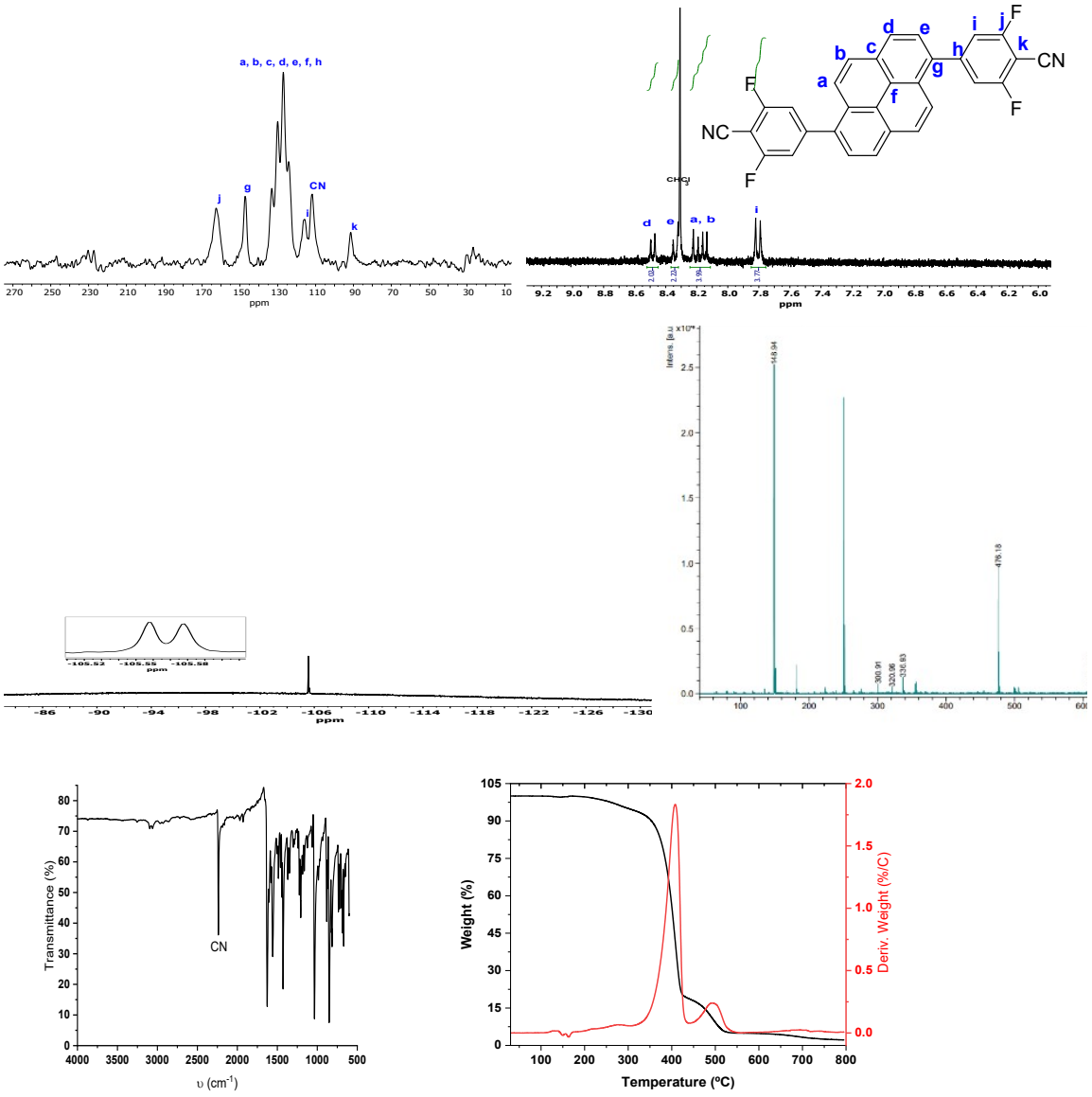

Figure S3. ^{1}H-NMR, ^{13}C-NMR, ^{19}F-NMR, ATR-IR, APCI-MS spectra and TGA of **3**.

3. Characterization of CTFs

Table S1. Elemental analysis

CTFs		C (%)	H (%)	N (%)
1,6-Pyr-CTF	Calc.	84.3	4.42	10.9
	Found	78.4	4.40	8.80
1,6-DPhPyr-CTF	Calc.	88.2	4.94	6.86
	Found	79.4	4.89	5.91
1,6-2FDPhPyr-CTF	Calc.	74.42	2.73	7.14
	Found	68.31	2.73	6.22

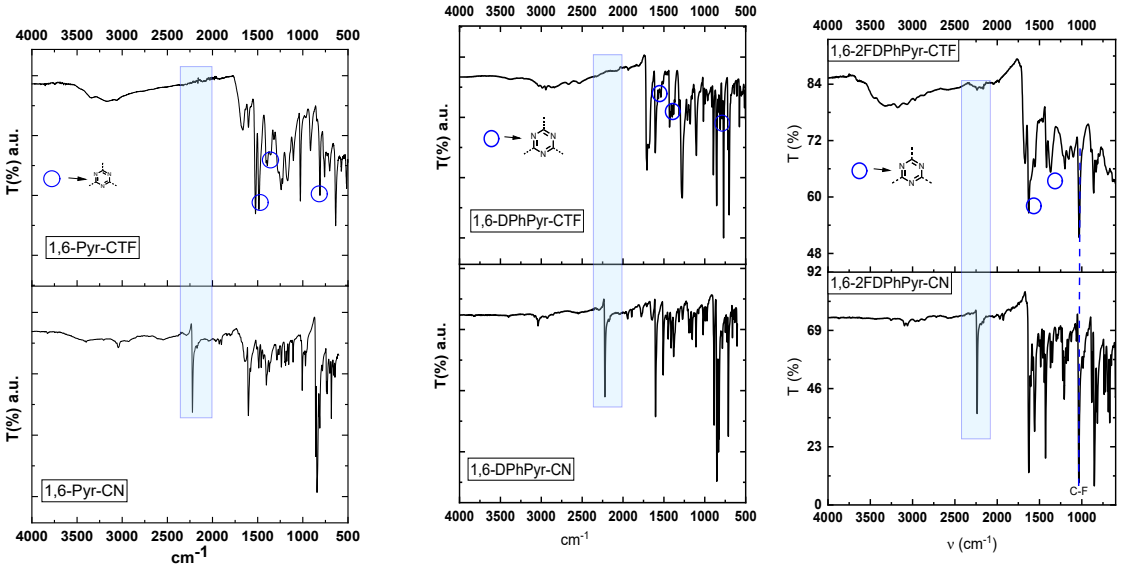

Figure S4. ATR-IR of 1,6 pyrene-based CTFs compared with the corresponding dinitriles

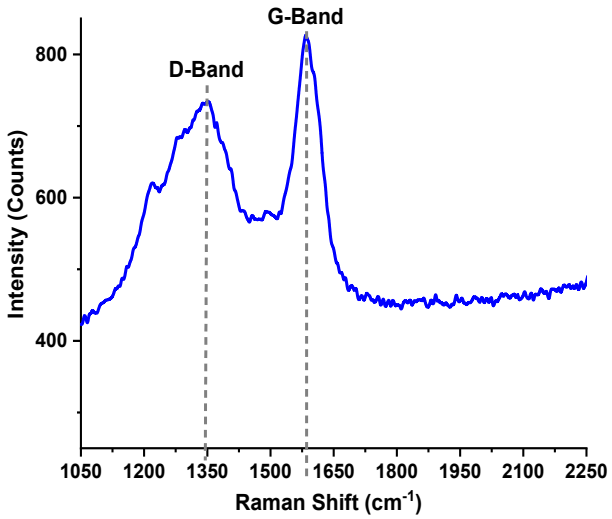

Figure S5. Raman spectrum of 1,6-2FDPhPyr-CTF.

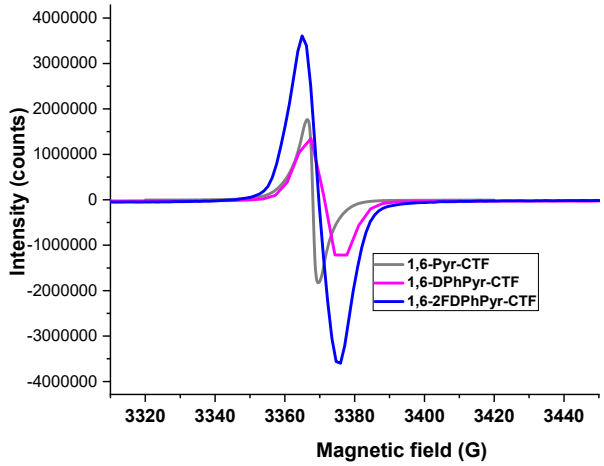

Figure S6. EPR spectra of 1,6 pyrene-based CTFs.

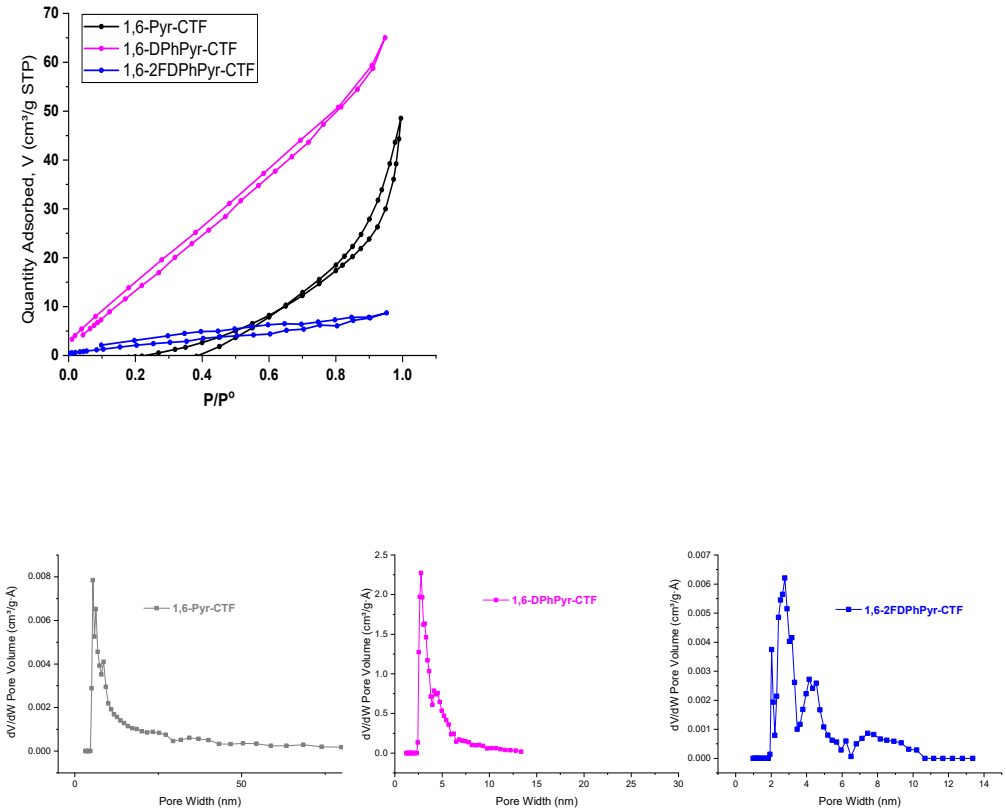

Figure S7. N_2 adsorption-desorption isotherms (*top*) and pore distribution by DFT method (*down*) of 1,6-pyrene-based CTFs.

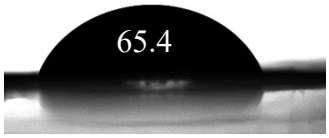

Figure S8. Water contact angle of 1,6-2FDPhPyr-CTF.

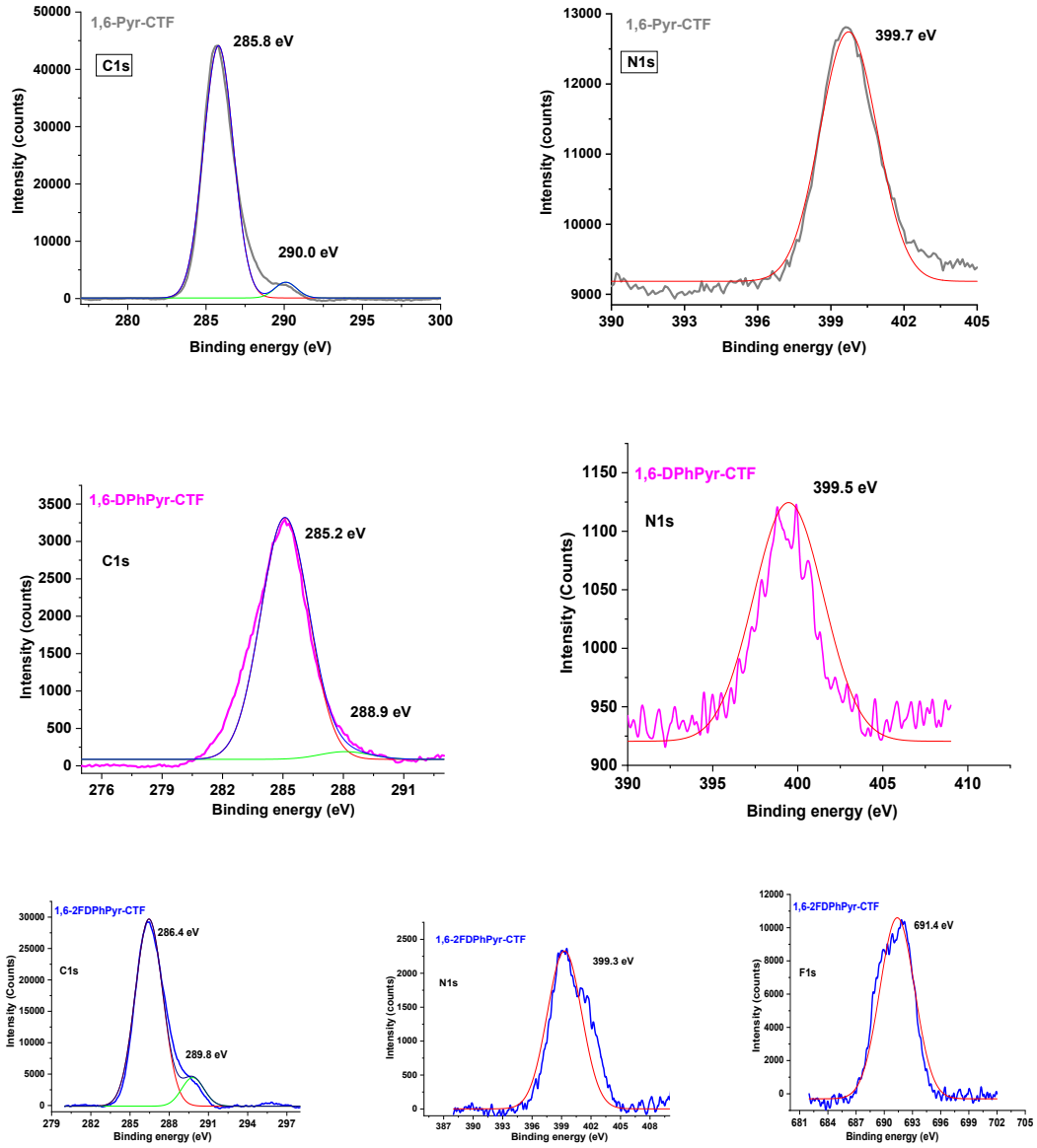

Figure S9. XPS C1s, N1s and F1s traces of 1,6 pyrene-based CTFs.

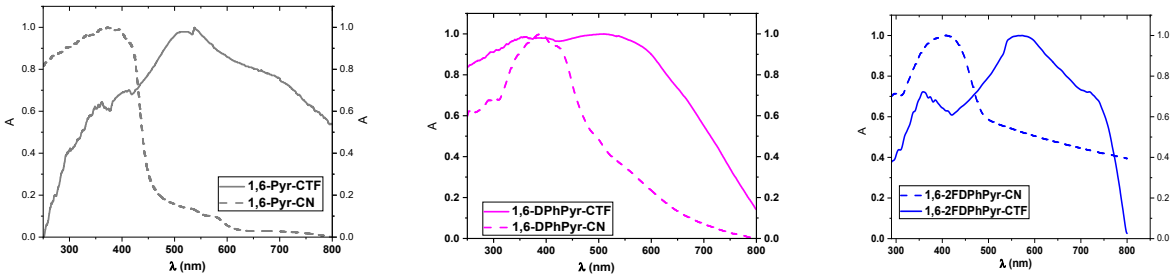

Figure S10. Comparison of solid-state UV-Visible spectra of the parent dinitriles and their corresponding covalent triazine frameworks (CTFs).

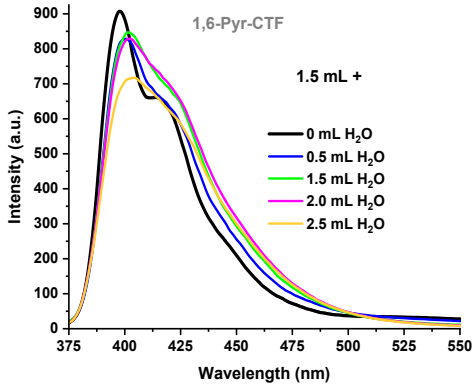

Figure S11. 1,6-Pyr-CTF: Emission spectra dispersed in EtOH-H_2O mixtures ($\lambda_{exc.}$ = 355 nm).

4. Sensing experiments

4.1. Detection of nitroaromatic compounds

The detection sensitivity was studied by fluorescence quenching Stern−Volmer constants (K_{SV}) and detection limits. **K_{SV}** values were obtained through the Stern−Volmer equation: $I_0/I = 1 + K_{SV}[NAC]$, where I_0 and I are the fluorescence intensity before and after adding the analyte, [NAC] is the analyte concentration and K_{SV} is the quenching coefficient. After each addition of analyte, the samples were sonicated for 10 seconds, the measurements were repeated at least 3 times, and the average values were selected in order to eliminate potential instrumental errors. In addition, every titration was repeated 3 times with different suspensions and we have obtained the standard deviation of I_0/I-1 for each concentration used to calculate the Stern-Volmer constants. The ratios of I_0/I are plotted as a function of the analyte concentrations, then, the limits of detection (**LOD**) were calculated according to the equation LOD = 3σ/K, (σ is the standard error of fluorescence intensity of blank measurements of polymers suspension and ρ is slope of the calibration curve

(relative fluorescent intensity versus sample concentration). The σ of blank (n=10) was calculated for suspensions of **Pyr-CTFs** with values of σ=0.0031 (1,6-Pyr-CTF), σ=0.0077 (1,6-2FDPhPyr-CTF), σ=0.0046 (1,6-2FDPhPyr-CTF). **The quenching efficiency (QE)** was calculated by using the equation: $QE=(I_0-I)/I0 \times 100\%$, where I_0 is the initial fluorescence intensity and I is the fluorescence intensity in the presence of a concentration of the corresponding analyte.

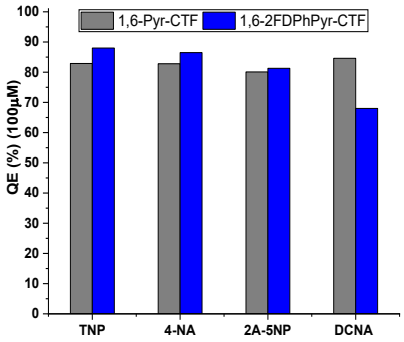

Figure S12. QE (%) of 1,6-pyrene based CFTs with different analytes at 100 μM.

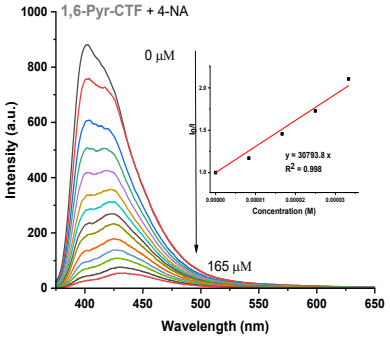
1,6-Pyr-CTF + 4-NA
0 μM
165 μM
Intensity (a.u.)
Wavelength (nm)
y = 30793.8 x
R2 = 0.998
Concentration (M)

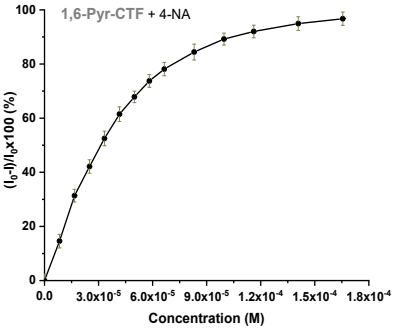
1,6-Pyr-CTF + 4-NA
(I0-I)/I0x100 (%)
Concentration (M)

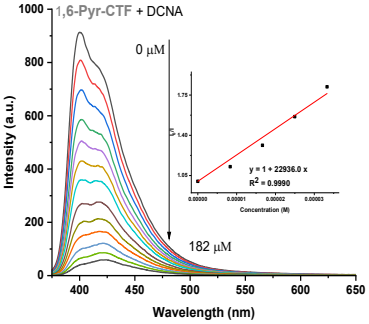
1,6-Pyr-CTF + DCNA
0 μM
182 μM
Intensity (a.u.)
Wavelength (nm)
y = 1 + 22936.0 x
R2 = 0.9990
Concentration (M)

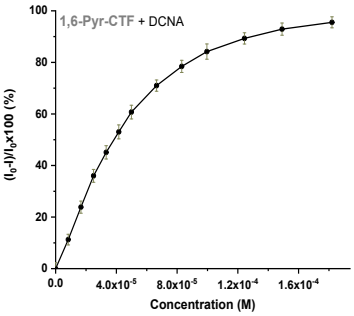
1,6-Pyr-CTF + DCNA
(I0-I)/I0x100 (%)
Concentration (M)

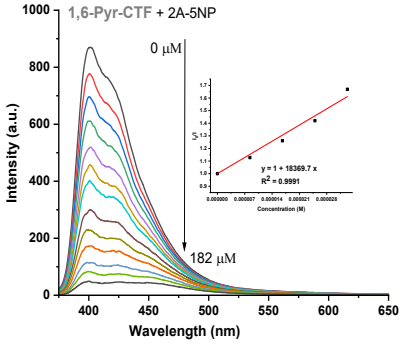
1,6-Pyr-CTF + 2A-5NP
0 μM
182 μM
Intensity (a.u.)
Wavelength (nm)
y = 1 + 18369.7 x
R2 = 0.9991
Concentration (M)

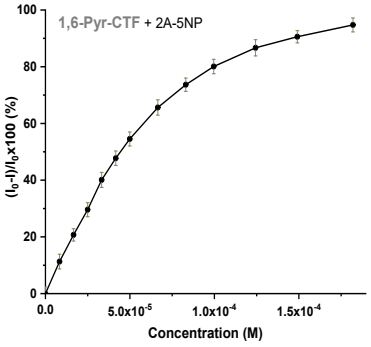
1,6-Pyr-CTF + 2A-5NP
(I0-I)/I0x100 (%)
Concentration (M)

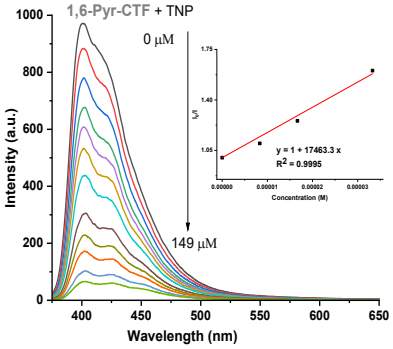
1,6-Pyr-CTF + TNP
0 μM
149 μM
Intensity (a.u.)
Wavelength (nm)
y = 1 + 17463.3 x
R2 = 0.9995
Concentration (M)

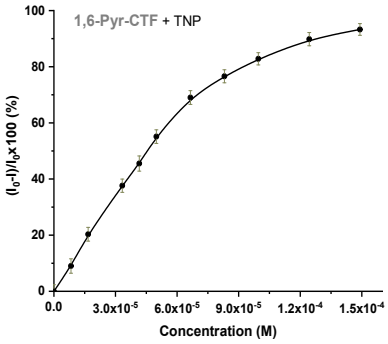
1,6-Pyr-CTF + TNP
(I0-I)/I0x100 (%)
Concentration (M)

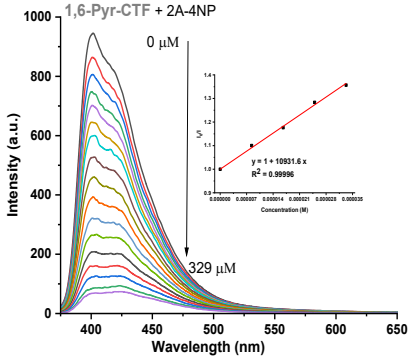
1,6-Pyr-CTF + 2A-4NP
0 μM
329 μM
y = 1 + 10931.6 x
R² = 0.99996
Concentration (M)
Intensity (a.u.)
Wavelength (nm)

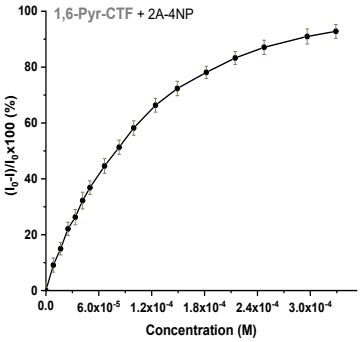
1,6-Pyr-CTF + 2A-4NP
(I0-I)/I0x100 (%)
Concentration (M)

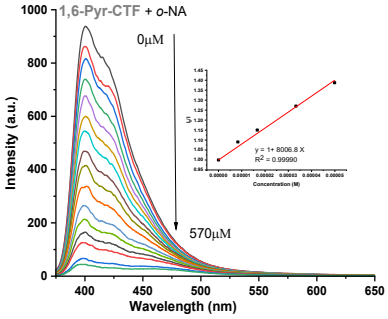
1,6-Pyr-CTF + o-NA
0μM
570μM
y = 1+ 8006.8 X
R² = 0.99990
Concentration (M)
Intensity (a.u.)
Wavelength (nm)

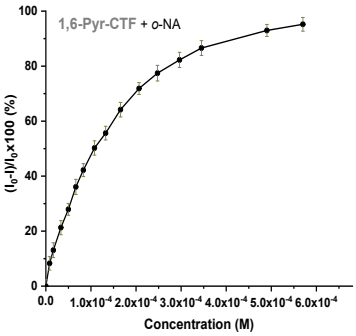
1,6-Pyr-CTF + o-NA
(I0-I)/I0x100 (%)
Concentration (M)

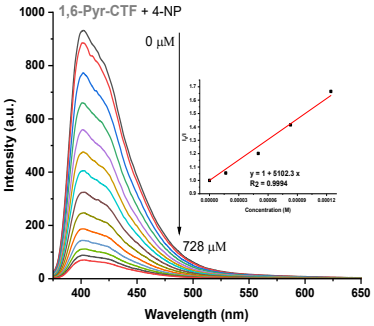
1,6-Pyr-CTF + 4-NP
0 μM
728 μM
y = 1 + 5102.3 x
R2 = 0.9994
Concentration (M)
Intensity (a.u.)
Wavelength (nm)

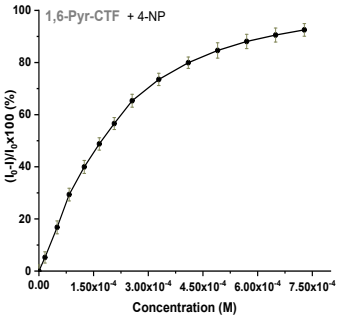
1,6-Pyr-CTF + 4-NP
(I0-I)/I0x100 (%)
Concentration (M)

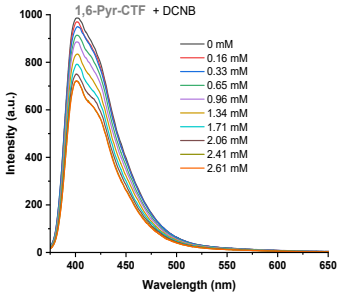
1,6-Pyr-CTF + DCNB
0 mM
0.16 mM
0.33 mM
0.65 mM
0.96 mM
1.34 mM
1.71 mM
2.06 mM
2.41 mM
2.61 mM
Intensity (a.u.)
Wavelength (nm)

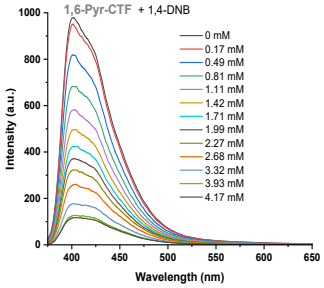
1,6-Pyr-CTF + 1,4-DNB
0 mM
0.17 mM
0.49 mM
0.81 mM
1.11 mM
1.42 mM
1.71 mM
1.99 mM
2.27 mM
2.68 mM
3.32 mM
3.93 mM
4.17 mM
Intensity (a.u.)
Wavelength (nm)

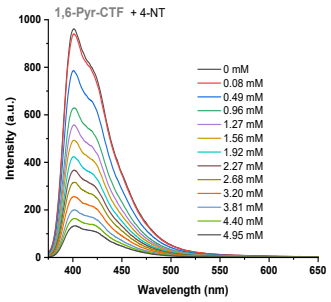
1,6-Pyr-CTF + 4-NT
0 mM
0.08 mM
0.49 mM
0.96 mM
1.27 mM
1.56 mM
1.92 mM
2.27 mM
2.68 mM
3.20 mM
3.81 mM
4.40 mM
4.95 mM
Intensity (a.u.)
Wavelength (nm)

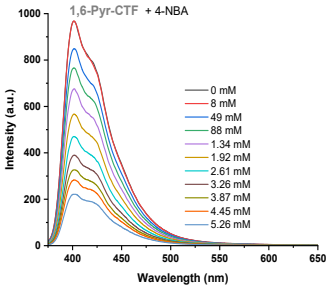
1,6-Pyr-CTF + 4-NBA
0 mM
8 mM
49 mM
88 mM
1.34 mM
1.92 mM
2.61 mM
3.26 mM
3.87 mM
4.45 mM
5.26 mM
Intensity (a.u.)
Wavelength (nm)

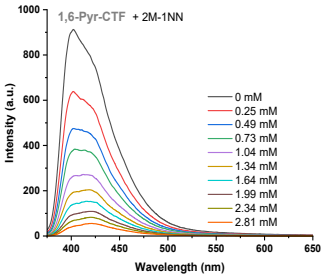
1,6-Pyr-CTF + 2M-1NN
0 mM
0.25 mM
0.49 mM
0.73 mM
1.04 mM
1.34 mM
1.64 mM
1.99 mM
2.34 mM
2.81 mM
Intensity (a.u.)
Wavelength (nm)

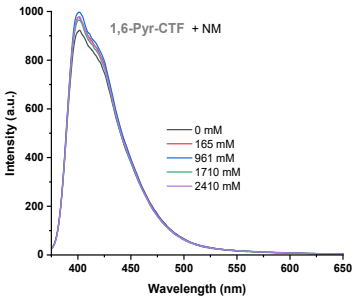
1,6-Pyr-CTF + NM
0 mM
165 mM
961 mM
1710 mM
2410 mM
Intensity (a.u.)
Wavelength (nm)

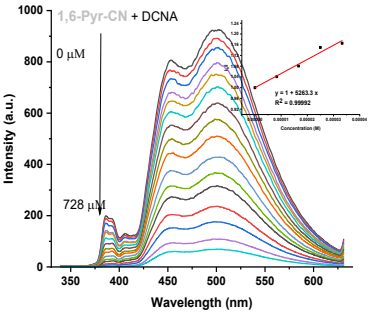
1,6-Pyr-CN + DCNA
0 μM
728 μM
y = 1 + 5263.3 x
R² = 0.99992
Concentration (M)
Intensity (a.u.)
Wavelength (nm)

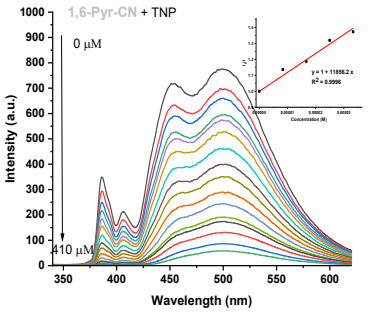
1,6-Pyr-CN + TNP
0 μM
410 μM
y = 1 + 11656.2 x
R² = 0.9996
Concentration (M)
Intensity (a.u.)
Wavelength (nm)

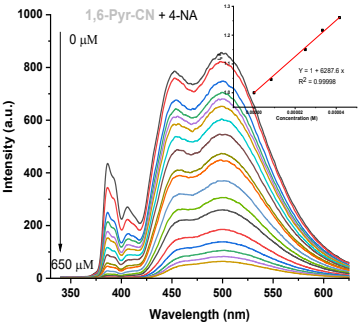
1,6-Pyr-CN + 4-NA
0 μM
650 μM
Y = 1 + 6287.6 x
R² = 0.99998
Concentration (M)
Intensity (a.u.)
Wavelength (nm)

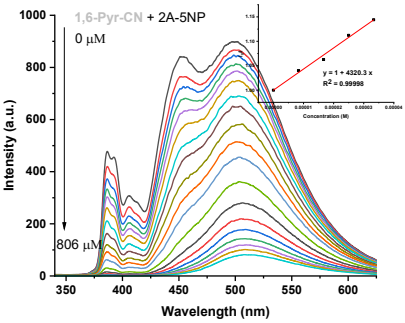
1,6-Pyr-CN + 2A-5NP
0 μM
806 μM
y = 1 + 4320.3 x
R² = 0.99998
Concentration (M)
Intensity (a.u.)
Wavelength (nm)

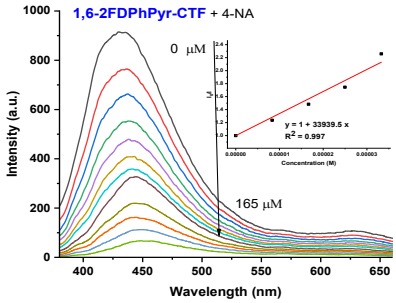
1,6-2FDPhPyr-CTF + 4-NA
0 μM
165 μM
y = 1 + 33939.5 x
R² = 0.997
Concentration (M)
Intensity (a.u.)
Wavelength (nm)

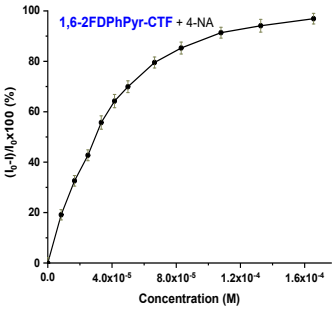
1,6-2FDPhPyr-CTF + 4-NA
(I0-I)/I0x100 (%)
Concentration (M)

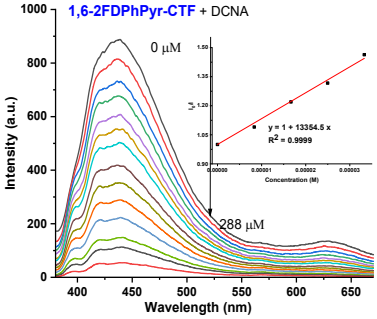
1,6-2FDPhPyr-CTF + DCNA
0 μM
288 μM
y = 1 + 13354.5 x
R² = 0.9999
Concentration (M)
Intensity (a.u.)
Wavelength (nm)

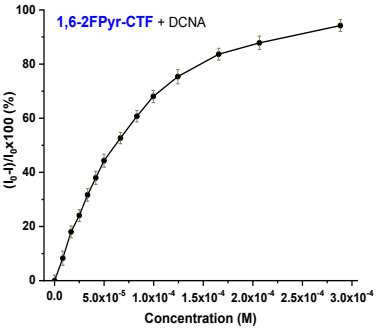
1,6-2FPyr-CTF + DCNA
(I0-I)/I0x100 (%)
Concentration (M)

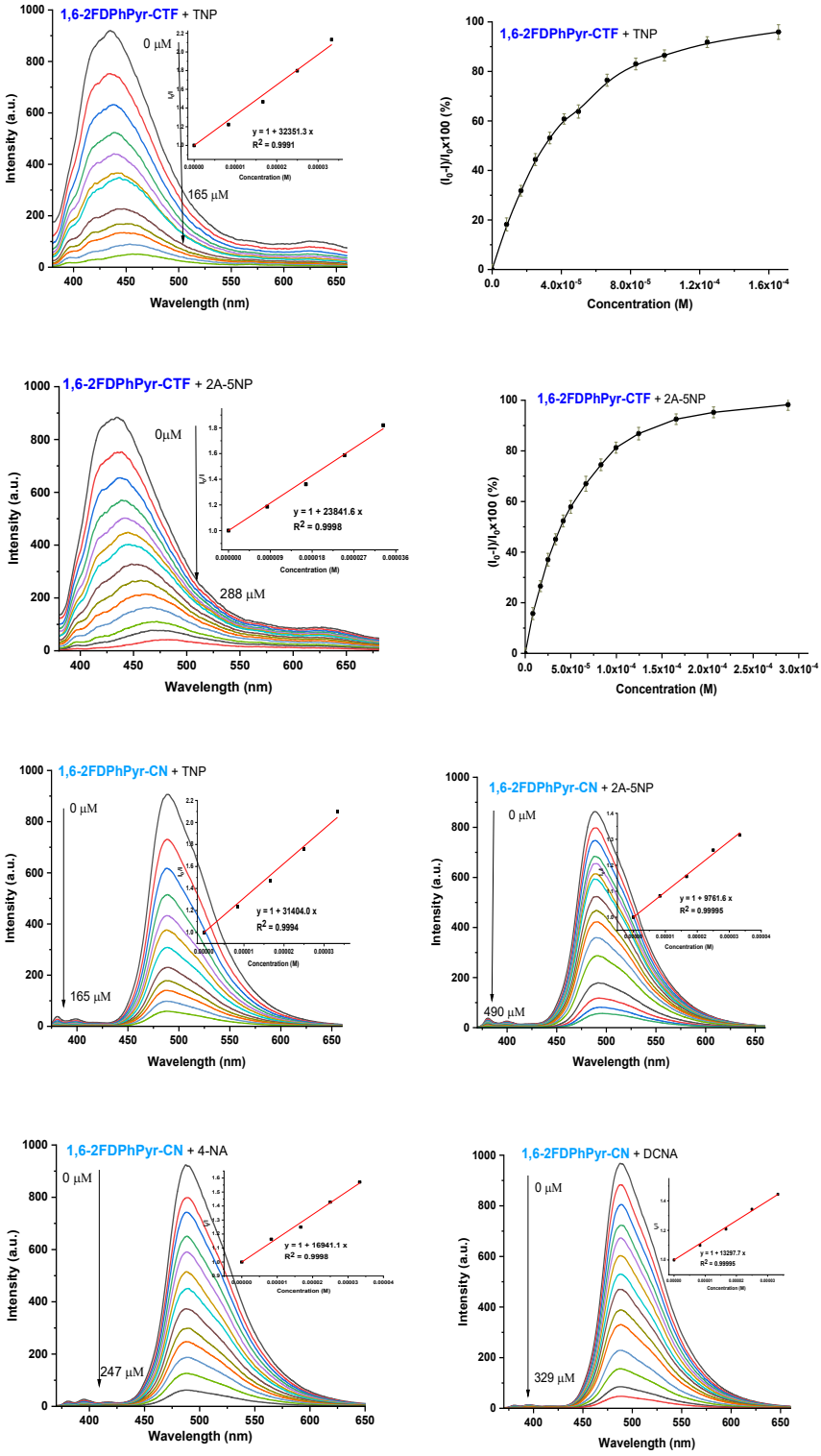

Figure S13. Fluorescence intensity of 1,6 pyrene-based CFTs and dinitriles as a function of analyte concentration.

Table S2. K_{SV} values, Quenching efficiencies (QE) (%) at 100 µM of Pyr-CTFs and limits of detection (LOD) in EtOH/H_2O of 1,6-Pyr-CTF and 1,6-2FDPhPyr-CTF.

Sensor	4-NA			2A-5NP		
	K_{SV} (M^{-1})	QE (%)[1]	LOD (ppm)	K_{SV} (M^{-1})	QE (%)[1]	LOD (ppm)
1,6-Pyr-CTF	30794	82.8	0.31	18370	80.1	0.16
1,6-2FDPhPyr-CTF	33939	86.5	0.11	23841	81.3	0.13
	TNP			DCNA		
	K_{SV} (M^{-1})	QE (%)[1]	LOD (ppm)	K_{SV} (M^{-1})	QE (%)[1]	LOD (ppm)
1,6-Pyr-CTF	17463	82.9	0.25	22936	84.5	0.18
1,6-2FDPhPyr-CTF	43549	88	0.15	14354	68.0	0.25

[1]At 100 µM.

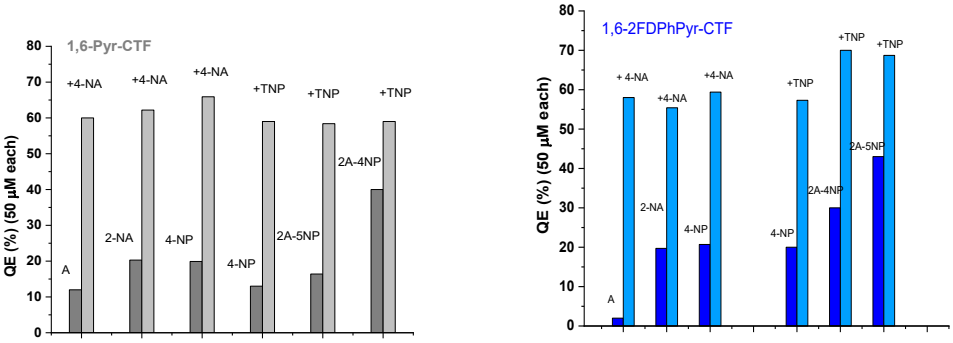

Figure S14. Selectivity studies of 1,6-Pyr-CTF and 1,6-2FDPhPyr-CTF.

5. Recovery of fluorescence

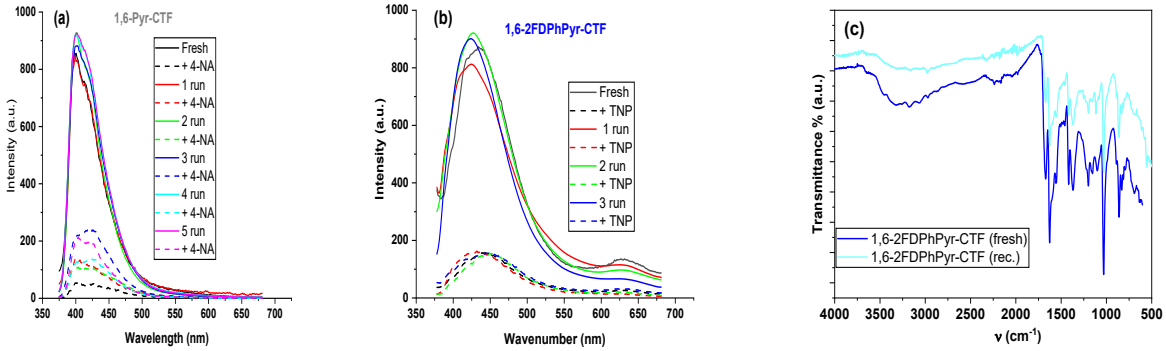

Figure S15. Recovery of fluorescence of (a)1,6-Pyr-CTF and (b) 1,6-2FDPhPyr-CTF. (c) IR spectra of recovered 1,6-Pyr-CTF and 1,6-2FDPhPyr-CTF after sensing experiments.

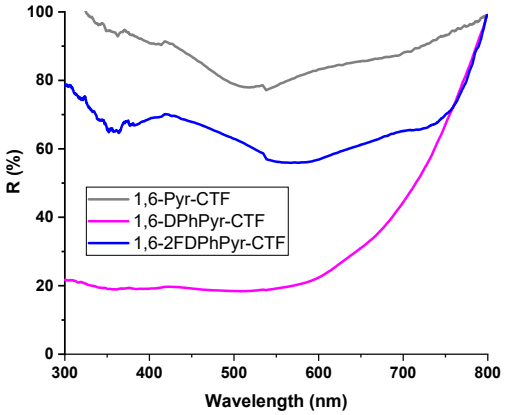

Figure S16. Diffuse reflectance spectra of 1,6-pyrene based CTFs.

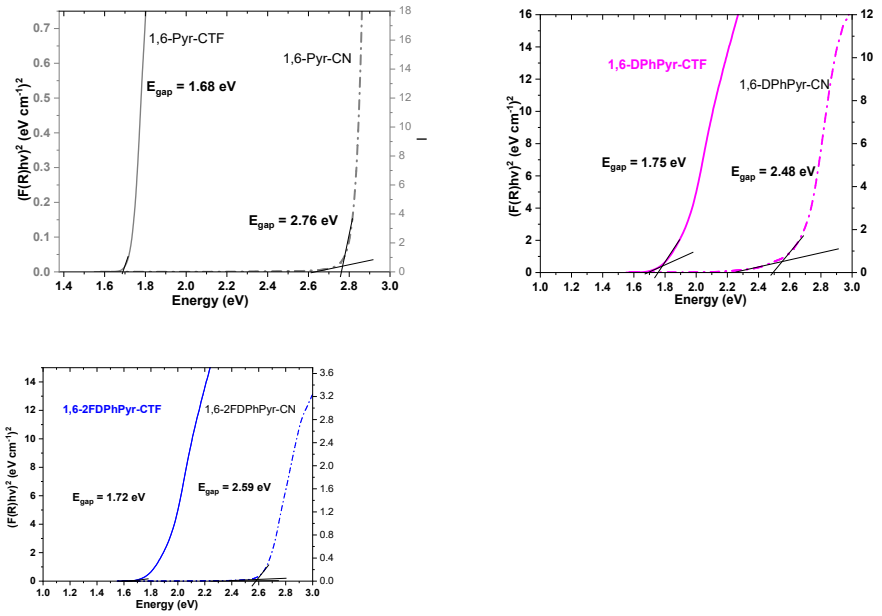

Figure S17. Tauc plots obtained from the Kubelka–Munk function of parent dinitriles and the corresponding 1,6-pyrene based CTFs.

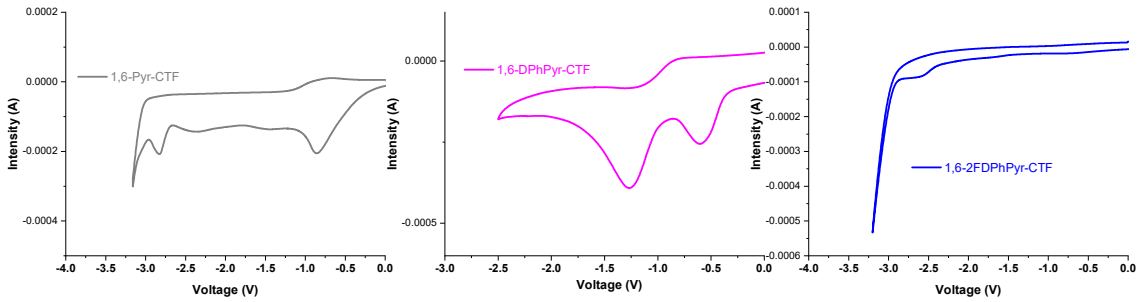

Figure S18. Cyclic voltammetry of 1,6 pyrene-based CTFs.

Table S3. Electrochemical properties of pyrene-CTFs.

Compound	E_{gap} (eV)[b]	E^{o}_{red} (V)	E_{LUMO} (eV)[c]	E_{HOMO} (eV)[d]
1,6-Pyr-CTF	1.68	-1.60	-2.635	-4.315
1,6-DPhPyr-CTF	1.75	-1.29	-2.945	-4.695
1,6-2FDPhPyr-CTF	1.72	-1.67	-2.565	-4.285

[a]Band gap calculated from tauc plot. [b]Calculated with the onset reduction potential from CV (E_{LUMO}= - [E_{red}^{onset} + U(Ag/AgCl 3.5M KCl/SHE) + 4.44] eV. [c]Estimated from $E_{LUMO} = E_{gap} + E_{HOMO}$.

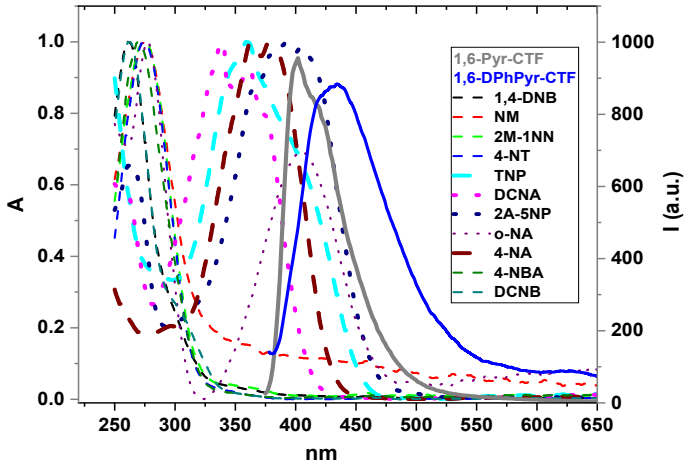

Figure S19. Absorption of NACs (dashed lines) and fluorescence emission (continuous lines) spectra of Pyr-CTFs.

Table S4. Summarized data for triazine-based small molecules and organic polymer frameworks (COFs and CTFs) for detection of TNP, 4-NA and DCNA.[6,7,8,9]

	Sensor	λ_{ex} (nm)	λ_{em} (nm)	Analyte	Solvent	LOD	K_{SV} (M^{-1})	Ref.
1	1,6-Pyr-CTF	355	400	TNP	H_2O/EtOH (1/1)	0.25 ppm	1.75×10^4	this work
2	1,6-2FDPhPyr-CTF	355	435	TNP	H_2O/EtOH (1/1)	0.15 ppm	4.35×10^4	
3	2,7-Pyr-CTF	340	525	TNP	DOX	0.49 ppm	$9.24x10^3$	[10]
4	2,7-4FDPhPyr-CTF	340	525	TNP	DOX	0.53 ppm	7.82×10^3	[10]
5	TZNET	398	448	TNP	H_2O/THF (90:10)	203 nM	1.02×10^3	[11]
6	SNW-1	370	467	TNP	H_2O/THF (90:10)	0.050 μM	9.46×10^4	[12]
7	TRZBT	430	527	TNP	H_2O/THF (90:10)	0.61 nM	4.91×10^5	[13]
8	HL-COF-1	419	495	TNP	H_2O	9.3 nM	1.20×10^5	[14]
9	T1	290	437	TNP	H_2O/DMF (4:1, v/v)	1.94 nM	1.07×10^6	[15]
10	TRZDPA	396	504	TNP	THF	0.37 nM	3.53×10^5	[16]
11	DTZ-COF	350	485	TNP	THF	81.8 ppb	8.71×10^4	[17]
12	TDPDB	390	~470	TNP	THF	1.93×10^{-5}μM	1.55×10^4	[18]
13	Py-azine COF	470	522	TNP	ACN		7.8×10^4	[19]
14	Py-azo-COP	415	485	TNP	THF		1.37×10^3	[20]
15	HHQ	260	325	TNP	THF	$1.3x10^{-5}$μM	2.30×10^5	[21]
16	TTPB	370	465	TNP	DOX	8.14×10^{-3} μM	1.29×10^3	[22]
17	TAPBDA	345	480	TNP	DOX	1.06×10^{-3}μM	2.82×10^4	[23]
18	TBN-1	365	490	TNP	DMF	0.15 ppm	$2.89x10^5$	[24]
19	TBP	393	450	TNP	DMF	$6.08x10^{-5}$μM	4.93×10^4	[25]
20	1,6-Pyr-CTF	375	400	4-NA	EtOH/H_2O (1/1)	0.31 ppm	3.08×10^4	this work
21	1,6-2FDPhPyr-CTF	375	435	4-NA	EtOH/H_2O (1/1)	0.11 ppm	3.39×10^4	
22	DPA-CTF	418	590	4-NA	EtOH	1.5 μM	$3.7x10^4$	[26]
23	EPO-CTF	394		4-NA	EtOH	0.91 μM	1.01×10^5	[27]
24	ANCOF	320	425	4-NA	MeOH/H_2O(1.5:0.5)	89 ppb	8.37×10^4	[28]
25	PCBTC	375	544	4-NA	DMF	21.5 nM	$4.95x10^6$	[29]
26	TPDC-DB	365	468	4-NA	THF	455 ppb	$1.70x10^4$	[30]
27	1,6-Pyr-CTF	375	400	DCNA	EtOH/H_2O (1/1)	0.18 ppm	2.29×10^4	this work
28	1,6-2FDPhPyr-CTF	375	435	DCNA	EtOH/H_2O (1/1)	0.25 ppm	1.43×10^4	
29	2,7-Pyr-CTF	340	525	DCNA	DOX	0.20 ppm	2.56×10^4	[10]
30	2,7-4FDPhPyr-CTF	340	525	DCNA	DOX	0.18 ppm	2.57×10^4	[10]
31	ANCOF	320	425	DCNA	MeOH/H_2O(1.5:0.5)	142 ppb	8.30×10^4	[28]
32	ACPP	365	500	DCNA	H_2O	7.9 ppb	3.80×10^5	[31]
33	LNU-45	365	475	DCNA	THF	0.0155 ppm	5.71×10^3	[32]
34	LNU-47	365	475	DCNA	THF	0.0197 ppm	2.88×10^3	[32]

Computational Methodology

Density Functional Theory (DFT) calculations were utilized in order to analyze the interactions between 1,6-Pyr-CTF with the nitroaromatic compounds. The 4-NA and 4-NP were chosen as representative cases. As a 1,6-Pyr-CTF model, we chose a molecular model that consists of a triazine core, which is further extended by three (dimethyl-triazinyl)-pyrene groups, as shown in Figure 8 of the manuscript. Initially, a conformational sampling was performed in order to identify the lowest energy aggregates between the nitroaromatic molecules and the 1,6-Pyr-CTF. The sampling of the non-covalent complexes between the polymer model and the nitroatomatic compounds was done with the CREST v3.0.2 utility program at the extended tight-binding level GFN-xTB of theory.[33,34,35] Subsequently, the most stable conformations are chosen and their energies are minimized with the r^{2}SCAN-3c[36] method, followed by single point energy calculations with the M06-L[37] and M06-2X functionals in combination with the def2-TZVPP[38] basis set. The most stable conformations are chosen for further optimization with the M06-L functional, followed by single point energy calculations at the M06L/def2-QZVPP level. The r-^{2}SCAN-3c and M06-L optimized geometries are confirmed to be minima after performing a harmonic frequency calculation. All DFT calculations are performed in the ORCA 6.0.1[39] code utilizing the DEFGRID-3 grid. The analysis of the interactions of 4-NA and 4-NP with the 1,6-Pyr-CTF models is performed at the M06-L/def2-QZVPP level by using the Interaction Region Indicator (IRI) method[40], as implemented within the Multiwfn 3.8(dev) wave function analysis code.[41]

Table S5: Binding energies (in kJ/mol) calculated from M06L/def2-QZVPP of the 4-NA and 4-NP with the 1,6-Pyr-CTF and 1,6-2FDPhPyr-CTF models. The presence of H-bonding between the hydroxo group of 4-NA/4-NP with the nitrogen atoms of the triazine ring or the fluoro atoms is also indicated.

Configuration	4-NP	H-bonding	4-NA	H-bonding
1,6-Pyr-CTF				
I	-58.8	YES (H…N)	-58.3	NO
II	-52.1	NO	-58.2	YES (H…N)
III	-51.0	NO	-58.1	YES (H…N)
IV	-48.1	NO	-58.4	NO
V	-43.9	YES (H…N)		
VI	-48.5	NO		
1,6-2FDPhPyr-CTF				
I	-50.8	YES (H…N)	-53.9	YES (H…F)
II	-50.8	YES (H…F)	-47.9	YES (H…N)

6. References

[1] A. G. Crawford, Z. Liu, I. A. I. Mkhalid, M. H. Thibault, N. Schwarz, G. Alcaraz, A. Steffen, J. C. Collings, A. S. Batsanov, J. A. K. Howard and T. B. Marder. *Chem. Eur. J.* 2012, **18**, 5022−5035. http://dx.doi.org/10.1002/chem.201103774.

[2]. P. Lillo, O. Cañadas, R. E. Dale and A. U. Acuña. *Biochemistry* 2002, **41**, 12436–12449. https://doi.org/10.1021/bi0261793.

[3] R. E. M. Diederix, C. Dávila, R. Giraldo and M. P. Lillo, *FEBS J.* 2008, **275** (21), 5393–5407. https://doi.org/10.1111/j.1742-4658.2008.06669.x.

[4](a) F.-W. Yen, Ch.-H. Chang Miaoli US 10,636,977 B2, Apr 28 2020; (b) Samsung Display-Kr2015/29430, 2015, A, Cn107652307, 2018, A, Valiant - CN105131938, 2017, B; (c) F. Li, M. Pan, Q. He, Q. Zhou, Q. Tang, Ch. Gong *Dyes Pigm.* 2022, 110203, https://doi.org/10.1016/j.dyepig.2022.110203

[5] (a) T.-M. Geng, C. Zhang, Ch. Hu, M. Liu, Y.-T. Fei and H.-Y. Xia *New J. Chem*., 2020, **44**, 2312 DOI: 10.1039/c9nj05509f. (b) X. Gong, X. Xie, N. Chen, Ch. Zheng, J. Zhu, R. Chen, W. Huang, D. Gao *Chin. J. Chem.* 2015, **33**, 967—973 https://doi.org/10.1002/cjoc.201500385, (c) X. Gong, D. Heeran, Q. Zhao, Ch. Zheng, D. S. Yufit, G. Sandford, D. Gao *Asian J. Org. Chem*. 2019, **8**, 722 – 730 https://doi.org/10.1002/ajoc.201900018

[6] G. Sathiyan, G. Venkatesan, S. K. Ramasamy, J. Lee and S. Barathi, *J. Environ. Chem. Eng.* 2024, **12**, 112804. https://doi.org/10.1016/j.jece.2024.112804.

[7] T. Skorjanc, D. Shetty and M. Valant. *ACS Sens.* 2021, **6**, 1461–1481. https://doi.org/10.1021/acssensors.1c00183.

[8] W. He, J. Duan, H. Liu, C. Qian, M. Zhu, W. Zhang and Y. Liao. *Progress in Polymer Science*, 2024, **148**, 101770. https://doi.org/10.1016/j.progpolymsci.2023.101770.

[9] E. V. Verbitskiy, G. N. Lipunova, E. V. Nosova and V. N. Charushin. *Dyes Pigm.* 2025, **240**, 112848. https://doi.org/10.1016/j.dyepig.2025.112848

[10] M. C. Borrallo-Aniceto, B. Fuerte-Díez, A. Valverde-González, L. González-Aguilera, M. L. Ferrer, M. P. Lillo, U. Díaz, E. M. Maya, M. Iglesias, *Mater. Today Chem.* 2025, **50**, 103149 https://doi.org/10.1016/j.mtchem.2025.103149

[11] H. Muniyasamy, C. Chinnadurai, M. Nelson, A. Veeramanoharan, M. Sepperumal and S. Ayyanar, *Ind. Eng. Chem. Res.* 2021, **60**, 7987–7997. https://doi.org/10.1021/acs.iecr.1c00827

[12] W. Zhang, L. G. Qiu, Y. P. Yuan, A. J. Xie, Y. H. Shen and J. F. Zhu, *J. Hazard. Mater*. 2012, **221–222**, 147–154. https://doi.org/10.1016/j.jhazmat.2012.04.025.

[13] G. Sathiyan, D. Mathivanan, B. Bhuvaneshwari, A. Garg, R. K. Gupta and A. Singh, *Sens. Actuators A: Phys.*, 2021, **331**, 113026. https://doi.org/10.1016/j.sna.2021.113026.

[14] Y. Zhang, D. Wei, W. Zhang, Y. Zhao, X. Luo and H. Li, *Macromol. Rapid Commun.* 2025, **46**, 2400673. https://doi.org/10.1002/marc.202400673.

[15] F. Munir, M. T. Waseem, Z. A. Khan, S. Majeed, U. Farooq and S. A. Shahzad, *J. Photochem. Photobiol. A Chem.* 2022, **429**, 113921. https://doi.org/10.1016/j.jphotochem.2022.113921.

[16] G. Sathiyan, B. Balasubramaniam, S. Ranjan, S. Chatterjee, P. Sen, A. Garg, R. K. Gupta and A. Singh, *Mater. Today Chem.* 2019, **12**, 178–186. https://doi.org/10.1016/j.mtchem.2019.01.002.

[17] Y. Li, Y. Han, M. Chen, Y. Feng and B. Zhang, *RSC Adv.* 2019, **9**, 30937–30942. https://doi.org/10.1039/c9ra06583k.

[18] T. Geng, M. Liu, C. Zhang, C. Hu and H. Y. Xia, *Polym. Adv. Technol.* 2020, **31**, 1388–1394. https://doi.org/10.1002/pat.4868.

[19] S. Dalapati, S. Jin, J. Gao, Y. Xu, A. Nagai and D. Jiang. *J. Am. Chem. Soc.* 2013, **135**, 17310−172013. https://doi.org/10.1021/ja4103293.

[20] S. K. Gupta, D. Kaleeswaran, S. Nandi, R. Vaidhyanathan and R. Murugavel, *ACS Omega*, 2017, **2**, 3572–3582. https://doi.org/10.1021/acsomega.7b00515.

[21] T. M. Geng, M. Liu, C. Hu and H. Zhu, *New J. Chem.* 2021, **45**, 3007–3013. https://doi.org/10.1039/d0nj06099b.

[22] T. Geng, Z. Zhu, W. Zhang and Y. Wang, *J. Mater. Chem. A* 2017, **5**, 7612–7617. https://doi.org/10.1039/c7ta00590c.

[23] K. Wang, T. M. Geng, H. Zhu and C. Guo, *Micropor. Mesopor. Mat.*, 2024, **363**, 112794.

https://doi.org/10.1016/j.micromeso.2023.112794
[24] H. Shan, J. Jiao, Y. Du, Y. Li, R. Zhang, D. Cai and P. Qin, *Sep. Purif. Technol.,* 2024, **344**, 127208. https://doi.org/10.1016/j.seppur.2024.127208
[25] T. M. Geng, C. Hu, M. Liu and H. Y. Xia, *Spectrochim. Acta A Mol. Biomol. Spectrosc.*, 2021, **258**, 119852. https://doi.org/10.1016/j.saa.2021.119852.
[26] H. Hong, N. Wu, M. Han, Z. Guo, H. Zhan, S. Du and B. Chen, *Mater. Chem. Front.* 2021, **5**, 6568–6574. https://doi.org/10.1039/d1qm00686j.
[27] N. Wu, R. Jia, H. Hong, H. Gao, Z. Guo, H. Zhan, S. Du and B. Chen, *Polymer*, 2022, **246**, 124752. DOI: 10.1016/j.polymer.2022.124752.
[28] P. Das, G. Chakraborty and S. K. Mandal, *ACS Appl. Mater. Interfaces* 2020, **12**, 10224–10232.. https://doi.org/10.1021/acsami.9b17452.
[29] D. Zhang, F. Xu, Q. Lu, R. Zhang and J. Xia *Eur. Polymer J.*, 2023, **194**, 112110. https://doi.org/10.1016/j.eurpolymj.2023.112110.
[30] A. Deshmukh, S. Bandyopadhyay, A. James and A. Patra, *J. Mater. Chem. C*, 2016, **4**, 4427–4433. https://doi.org/10.1039/C6TC00599C.
[31] G. Yu, Z. Zhang, Y. Ling, J. Sun. *Dyes Pigm.* 2024, **222**, 111834. https://doi.org/10.1016/j.dyepig.2023.111834
[32] Z. Yan, J. Liu, C. Miao, P. Su, G. Zheng, B. Cui, T. Geng, J. Fan, Z. Yu, N. Bu, Y. Yuan and L. Xia, *Molecules* 2022, **27**, 126. https://doi.org/10.3390/molecules27010126.
[33] P. Pracht, S. Grimme, C. Bannwarth, F. Bohle, S. Ehlert, G. Feldmann, J. Gorges, M. Müller, T. Neudecker, C. Plett, S. Spicher, P. Steinbach, P.A. Wesołowski, F. Zeller, *J. Chem. Phys.* 2024, **160**, 114110. https://doi.org/10.1063/5.0197592.
[34] C. Bannwarth, S. Ehlert, S. Grimme, *J. Chem. Theory Comput.* 2019, **15**, 1652–1671. https://doi.org/10.1021/acs.jctc.8b01176.
[35] C. Bannwarth, E. Caldeweyher, S. Ehlert, A. Hansen, P. Pracht, J. Seibert, S. Spicher, S. Grimme, *WIREs Computational Molecular Science*. 2021, **11**, e1493. https://doi.org/https://doi.org/10.1002/wcms.1493.
[36] S. Grimme, A. Hansen, S. Ehlert, J.-M. Mewes, *J. Chem. Phys.* 2021, **154**, 64103. https://doi.org/10.1063/5.0040021.
[37] Y. Zhao, D.G. Truhlar, *J. Chem. Phys.* 2006, **125**, 194101. https://doi.org/10.1063/1.2370993.
[38] F. Weigend, R. Ahlrichs, *Phys. Chem. Chem. Phys.* 2005, **7**, 3297–3305. https://doi.org/10.1039/B508541A.
[39] F. Neese, Software update: The ORCA program system—Version 5.0, *WIREs Computational Molecular Science*. 2022, **12**, e1606. https://doi.org/https://doi.org/10.1002/wcms.1606.
[40] T. Lu, Q. Chen, *Chemistry–Methods*. 2021, **1**, 231–239. https://doi.org/https://doi.org/10.1002/cmtd.202100007.
[41] T. Lu, *J. Chem. Phys.* 2024, **161**, 82503. https://doi.org/10.1063/5.0216272.